

Ultrafast Intramolecular Electron Transfer Studied by Picosecond and Stationary Raman Spectroscopy

Wolfgang Werncke,* Sebastian Wachsmann-Hogiu,# Jens Dreyer, Alexander Ivanovich Vodchits,† and Thomas Elsaesser

Max-Born-Institut für Nichtlineare Optik und Kurzzeitspektroskopie, Max-Born-Strasse 2A, D-12489 Berlin, Germany

†B.I. Stepanov Institute of Physics, Fr. Scaryna Ave. 68, Minsk 220072, Belarus

(Received October 1, 2001)

Ultrafast photoinduced intramolecular electron transfer (ET) of betaine-30 (B-30) is studied in different solvents by resonance Raman spectroscopy. We apply stationary and picosecond time-resolved Raman techniques combined with ab initio Hartree–Fock calculations. Picosecond Raman spectroscopy of the first excited singlet state allows to monitor changes of vibrational frequencies due to ET. From the intense Raman lines of the stationary resonance Raman spectra we predict relevant geometric changes of B-30 due to ET which are confirmed by calculations of geometrical changes between the ground and excited electronic states of B-30. The torsional motion between the phenolate and the pyridinium rings as well as nitrogen pyramidalization play an essential role in electron transfer. Vibrational modes accepting the bulk of excess energy after back-electron transfer are identified by time-resolved anti-Stokes resonance Raman spectroscopy. In particular, the highest-frequency mode of the resonance Raman spectrum exhibiting a large Franck–Condon factor is most effective in accepting energy. Mode specific excitation of B-30 after back-electron transfer results in non-equilibrium vibrational populations within the first few picoseconds and subsequent quasi-equilibrium populations of hot Raman active modes. The observed vibrational kinetics can be qualitatively understood by a solvent dependent interplay of direct vibrational excitation and intramolecular vibrational energy redistribution.

Photoexcitation of molecules generates a redistribution of charge density resulting in a non-equilibrium state with respect to intramolecular and environmental degrees of freedom. It is thus followed by intramolecular redistribution of vibrational energy (IVR) accompanied by geometry relaxation along the excited state reaction coordinate as well as solvent relaxation. In numerous nonadiabatic singlet photochemical reactions the electronic ground state is repopulated by internal conversion (IC) through conical intersections.[1] This process is enabled and promoted by coupling to vibrational modes. Numerical studies have shown that the consideration of only a few specific modes frequently provides at least a qualitatively correct understanding of the typically ultrafast dynamics of IC.[2] A minimum model includes three modes: (i) a tuning mode that provides the direction into the conical intersection by minimizing the energy gap between the two electronic states, (ii) a coupling mode having the appropriate symmetry to vibronically couple the two electronic states that renders the transition to be allowed, and (iii) an accepting mode which receives and quickly dissipates the excess energy from relaxation to prevent the back-reaction.[3] While theoretical studies have been successful in identifying these active modes it is quite difficult to gain information about active modes from experiments. However, if IVR rates are slow compared to the primary excitation rates strong non-equilibrium energy distributions within the vibrational manifold may actually be observed. Here, a combination of different techniques of resonance Raman spectroscopy provides a suitable methodology.

Stationary resonance Raman spectroscopy allows to analyze the electronic transition, e.g., to identify the Franck–Condon (FC) active modes, and to determine mode-specific displacements of the vibrational potentials upon excitation and thereby vibrational reorganization energies.[4–5] The displacements can be converted into normal mode elongations and thus provide information about molecular geometry changes shortly after excitation that is as long as the molecule is in the FC-region.[7,8] Time-resolved resonance Raman spectroscopy (on a pico- or subpicosecond time scale) can monitor the vibrational Raman spectrum of the electronically excited state. Finally, time-resolved anti-Stokes Raman spectroscopy is a particular sensitive probe of excited vibrational levels. By this means vibrational populations and their kinetics after electronic excitation and subsequent IC can be measured directly.[9,10]

Photoinduced electron transfer (ET) represents one of the most frequently encountered elementary photo chemical reactions occurring in small ion pairs as well as in large biological systems, e.g., in photosynthetic antenna systems. Accordingly, analysis and control of ET reactions has developed into a very active research area in physical chemistry.[11–13] Here, we study betaine-30 (B-30) as a prototypical example of a molecule undergoing ultrafast photoinduced intramolecular ET. Dipole moments of about 16 D in the electronic ground state (S_0) and 6 D in the S_1 state have been measured.[14] Consequently, the S_0

Present address: Carnegie Mellon University, Mellon Institute Box 154, 4400 Fifth Ave, Pittsburgh, PA 15213, USA

state is much more sensitive to changes of solvent polarity than the excited state. This results in a strong solvent dependence of the longest wavelength absorption band (CT band) located between 800 and 500 nm. This dependence has been used to characterize solvent polarities by the popular ET^{30}-scale.[15] The back-electron transfer (b-ET) reaction is very fast with rates depending mainly on temperature and the dynamic properties of the solvent. According to femtosecond time-resolved absorption measurements of Barbara and co-workers b-ET times ($\tau_{b\text{-}ET}$) at room temperature vary from 0.6 ps up to about 100 ps in different solvents.[16–18] It has been suggested that these transfer times are mainly controlled by the torsion between the phenolate and the pyridinium ring of the molecule modulating the gap between the S_1 and S_0 potentials.[19] However, the activity of the corresponding vibrational mode as a tuning mode remains to be shown.

In this paper we derive information about the molecular geometry and structural changes after photoinduced ET from stationary and time-resolved resonance Raman spectra accompanied by ab initio calculations. We identify the Raman active vibrational band in the resonance Raman spectrum which can be assigned to a tuning mode. We show which modes predominantly absorb excess energy after b-ET from the excited state back to the ground state resulting in strong non-equilibrium vibrational populations on a picosecond time scale and subsequently in enhanced temperatures of the subsystem of Raman active modes. Results are reported for solutions of B-30 with different solvation times.

Experimental

1. Stationary Vibrational Spectroscopy. B-30 and all solvents (spectral grade) were purchased from Aldrich and used without further purification. IR spectra of B-30 samples embedded in KBr were recorded with an FT-IR spectrometer (Biorad) between 400 and 1700 cm^{-1}. For stationary Raman measurements, B-30 was dissolved in propylene carbonate (PC), n-pentanol (PeOH), glycerol triacetine (GTA), dimethyl sulfoxide (DMSO), and ethanol (EtOH) with concentrations ranging from 2×10^{-2} M to 3×10^{-3} M. Resonance Raman spectra of B-30 were obtained by pulses of an average energy of 10 mW near 600 nm generated by a synchronously pumped dye laser with a spectral width of 8 cm^{-1}. The Raman spectra were recorded in quartz cells ($10 \times 10 \times 30$ mm^3) without stirring. The scattered light was imaged in a 135° back scattering geometry on the slit of the polychromator (SpectraPro 275, focal length 275 mm, with a 1200 lines/mm grating blazed at 500 nm for 600 nm excitation and with a 2400 lines/mm holografic grating for 300 nm excitation). Spectra were accumulated by a liquid nitrogen cooled CCD camera and accumulated typically in 100 s cycles. Integrated Raman intensities were determined — after subtraction of a base line — by fitting the Raman bands by Voigt line shapes.

2. Time-Resolved Raman Techniques. The picosecond time-resolved set-up for time-resolved Stokes and anti-Stokes Raman spectroscopy has been described elsewhere.[20] It is based on an amplified synchronously pumped dye laser system. The dye laser pulses were used for excitation of the first excited singlet state at 600 nm. For probing the Raman spectra pulses were frequency doubled to obtain radiation at 300 nm. For some experiments we used a cell filled with compressed methane at a pressure of 50 bar for shifting the 600 nm radiation by stimulated Raman scattering and subsequent frequency doubling.[21] Typical cross correlation widths between pump and probe pulses determined either by time-resolved stimulated transmission (e.g. time-resolved small signal amplification of a laser dye) or by time-resolved optical Kerr effect were about 5 ps (FWHM).

Time resolved Raman spectra were recorded in free flowing jets of 0.1 mm thickness (for EtOH and PC solutions) and of 0.3 mm thickness for the GTA, PeOH, and DMSO solutions. The probe pulse was polarized linearly at magic angle (54.7°) relative to the pump to avoid temporal changes of the Raman intensities due to molecular reorientation during delay time. For detection of the S_1 state we pumped the CT transition of B-30 near 600 nm. An S_1-S_n absorption band of B-30 around 400 nm has been reported. For resonance enhancement of S_1 we measured the pump induced Raman spectra at 370 nm. Using this excitation wavelength, scattering originating from molecules in the electronic ground state and from excited molecules contribute to the Raman spectra as well. We obtained the time resolved S_1 Raman spectra by subtracting from the pump induced Raman spectra the corresponding spectra recorded with pump pulses at a negative delay of 50 ps with respect to the probe pulse. Thus, depletion of the molecules in the electronic ground state manifests as negative dips in the Raman spectra and the positive contributions are due to the S_1 state.

For measuring vibrationally excited molecules generated after b-ET we used the same excitation at 600 nm, but recorded the pump induced anti-Stokes Raman spectra with 300 nm pulses. Raman probing at 300 nm results in strong resonance Raman enhancement of the vibrationally excited levels of the electronic ground state. Typical accumulation times for each spectrum at a fixed delay time were 100–200 s. Several spectra were averaged to obtain a sufficiently high signal to noise ratio.

Results

1. Optimized Geometries of Betaine-30. The ground-state molecular structure of B-30 shown in Fig. 1 has been optimized using Hartree-Fock ab initio calculations with a 3-21G

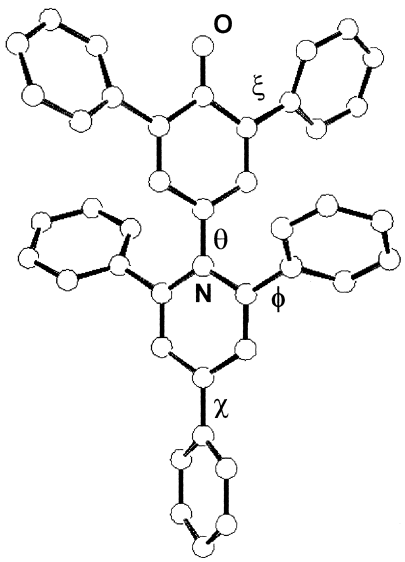

Fig. 1. HF/3-21G optimized molecular structure of B-30. θ, ξ and Φ are indicated and denote dihedral angles between the respective rings. For simplicity of illustration hydrogen atoms of the rings are not shown.

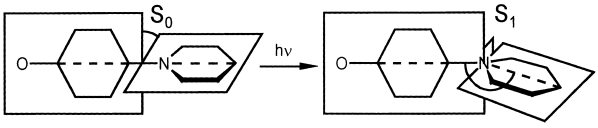

Fig. 2. Geometrical changes of B-30 between the electronic ground and first excited singlet following excitation of the CT transition.

basis set (HF/3-21G) implemented in the program package GAUSSIAN98.[22] The molecule exhibits C_2-symmetry with the C_2-axis oriented along the twisted chain of the phenolate, pyridinium and the bottom phenyl ring. The phenolate and pyridinium rings are twisted by $\theta = 68°$ and the bottom phenyl ring is twisted by $\chi = 45°$ with respect to the pyridinium ring. The calculated C–O bond length of 125.1 pm reveals a significant degree of double bond character. Accordingly, the adjacent C–C bonds of the phenolate ring are noticeably stretched in comparison to aromatic C–C bonds in benzene, and thus the phenolate ring structure exhibits some degree of quinoidal character. All other phenyl ring structures are nearly uniform.

To investigate principal geometry changes in the excited state CI-singles/6-31G(d) calculations for a reduced model system consisting solely of the phenolate and pyridinium rings were carried out. To be able to evaluate relative changes between the ground and the excited state the ground state model structure was optimized at the HF/6-31G(d) level as well. The most relevant geometry changes upon excitation to the first excited state are depicted schematically in Fig. 2.

The twisted conformation of the phenolate and pyridinium rings evolves into a perpendicular position, which has also been observed before.[19,23] In addition, the pyridinium ring tilts and the nitrogen atom becomes pyramidalized by $\lambda = 12°$.[24] Interestingly, the results for the model system of B-30 are nicely confirmed by recent CIS/3-21G calculations, in the gas phase as well as in solution (using self-consistent reaction field methods), for the complete B-30 molecule.[25]

2. Stationary Raman Spectroscopy of Betaine-30. A resonance Raman spectrum of B-30 dissolved in PC recorded with excitation within the charge transfer transition is shown in Fig. 3. A detailed assignment of the modes has been reported in Ref. 24. The spectrum exhibits strong lines in the finger print region which is in accordance with strong rearrangements of C–N, C–O and ring stretching and deformation motions due to ET. It is interesting to note that we also observe strong Raman lines in the low frequency region. The appearance of low-frequency Raman bands of similar intensity as the high-frequency modes is rather unusual as it demands for very strong origin shifts z between the electronic states. For strongly solvent-broadened charge transfer transitions $z \propto \sqrt{I_{Raman}/\omega_{Raman}}$ can be assumed (I_{Raman} – integrated Raman intensity of the line of frequency ω_{Raman}, $z = (m\omega_{Raman}/\hbar)^{1/2}q_0$ where m and q_0 are the effective mass and origin shift, respectively of the mode with frequency ω_{Raman}).[4] Consequently, the origin shift of the line at 133 cm^{-1} exceeds the origin shift of the 1603 cm^{-1} line nearly by an order of magnitude. According to our calculations the strongest low-frequency Raman lines at 133 cm^{-1} and 291 cm^{-1} are assigned to torsional and N-inversion motions of the skeleton, respectively.[24] Consequently, this enhancement supports the computational result that the rearrangement between the electronic states is mediated by the corresponding motions and the two strongest low-frequency Raman bands can be identified as tuning modes.

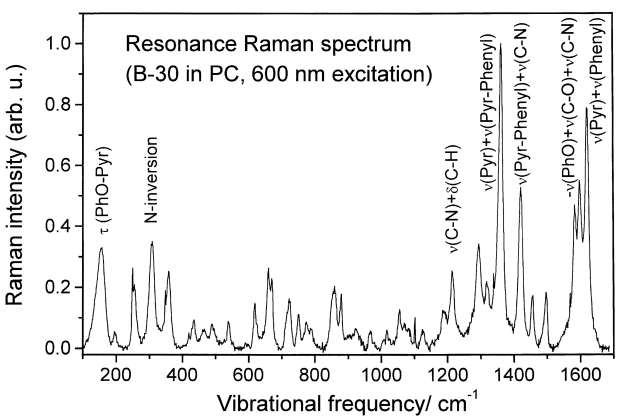

Fig. 3. Resonance Raman spectrum of B-30 dissolved in PC. Assignments of Raman lines are given in the insert.

3. Time Resolved Raman Spectra of the S_1-State of Betaine-30. Time-resolved Stokes–Raman spectra of the first excited singlet state after excitation of the CT transition were measured for B-30 dissolved in PeOH. PeOH has been selected as an appropriate solvent for such investigation because of the relatively long S_1 lifetime of B-30.[17,18] Figure 4a presents the S_0 Raman spectrum of B-30 with 364 nm laser excitation.

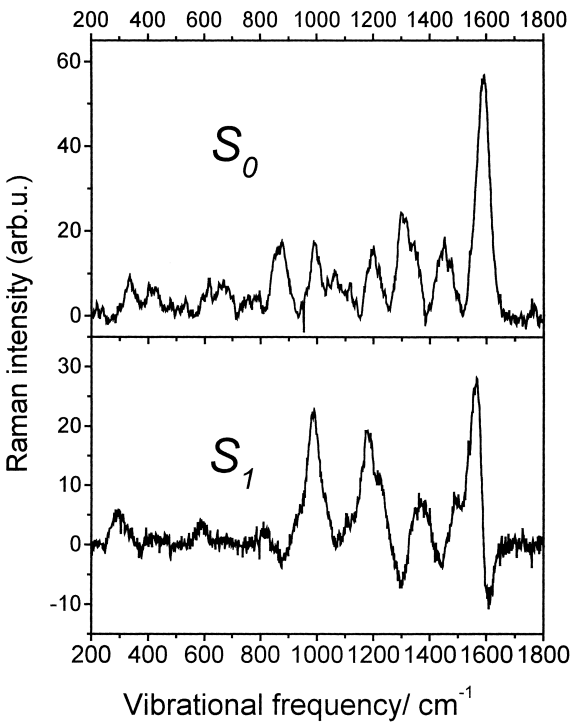

Fig. 4. (a) Stokes–Raman spectrum of the S_0 state of B-30 in PeOH with 364 nm excitation, and (b) of the S_1 state recorded with a pump wavelength of 600 nm and a probe at 364 nm. The time delay between the pump and the probe pulse is 5 ps.

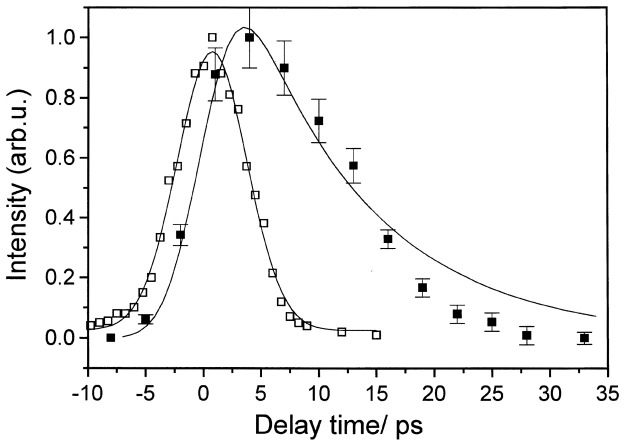

Fig. 5. Kinetics of the Stokes–Raman spectra in the S_1 state of B-30 dissolved in PeOH (solid squares) and cross-correlation between pump and probe pulses (open squares). The solid lines are the fits of the experimental points applying a two-level model.

In Fig. 4b, the pump induced S_1 Raman spectrum of B-30 dissolved in PeOH (after spectral subtraction of the S_0 spectrum as described in 2 section of Experimental) is shown. The negative contributions in the spectrum in Fig. 4b arise from the depletion of molecules in the electronic ground state by optical pumping.

As a representative example the change of intensity of one of the most prominent Raman bands at 1000 cm^{-1} with delay time between the pump and probe pulses is presented in Fig. 5. The other band intensities exhibit the same kinetics (not shown here). The experimental data were fit to a two-level model including the S_0 and S_1 states and taking a cross correlation time of this experiment of 6 ps into account. Thus, a decay time of the Raman intensity of 11 ps has been determined, which agrees with the lifetime of the S_1 state measured by Barbara et al. (11 ps) by transient absorption experiments.[17] The agreement in decay time provides evidence that the observed spectra originate from the excited electronic state of B-30. The S_1 Raman spectra of B-30 show significant intensity as well as frequency changes compared to the electronic ground state reflecting considerable alterations of the corresponding molecular geometries due to ET in its equilibrium geometry. Calculations of vibrational frequencies for an evaluation of the molecular structure on the basis of the excited state measurements are in progress.

4. Vibrational Excitation after Back-Electron Transfer of Betaine-30. Time-resolved anti-Stokes Raman spectra for 600 nm pump and 300 nm probe for B-30 dissolved in PC and GTA are shown in Figs. 6A and 6B, respectively. We detect a build-up of the anti-Stokes Raman lines within a few picoseconds predominantly in the high-frequency region. Subsequently, a decay accompanied by a redistribution of the relative intensities is observed. Later on, Raman lines at lower frequencies gain in their relative intensities with respect to the high-frequency Raman bands.

The anti-Stokes Raman lines agree with the strong Raman lines observed in the stationary Stokes Raman spectrum, but not with the Raman frequencies observed from the excited

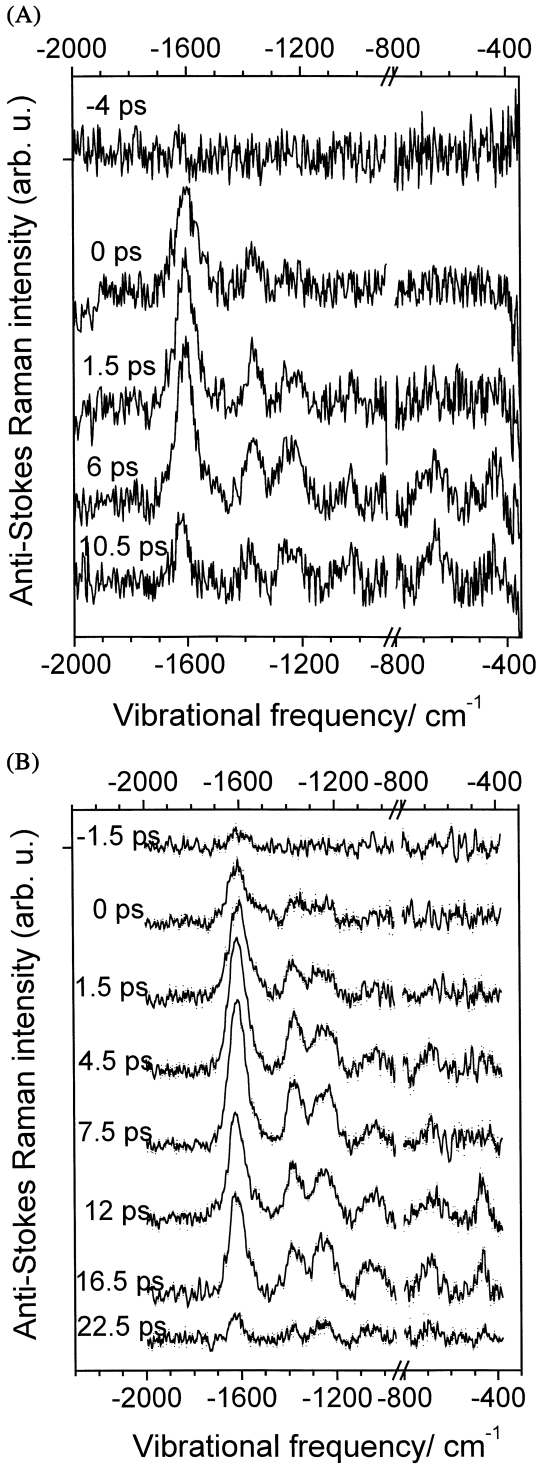

Fig. 6. Transient anti-Stokes Raman spectra of B-30 dissolved in PC (A) and GTA (B). Time delays between pump and probe pulses are indicated on the left side of each spectrum.

electronic state. Consequently, the rise and decay of the anti-Stokes Raman intensities reflect the population dynamics of excited vibrational levels of the electronic ground state after b-ET. For quantification the population dynamics of the vibrational level has been modeled by a three level model: an initially excited level with a decay time t_1, the first excited vibration-

Table 1. Rise (t_1) and Decay (t_2) Times (in ps) of anti-Stokes Raman Kinetic Curves Measured for B-30 Dissolved in PC, GTA, and EtOH. B-ET Times ($\tau_{b\text{-}ET}$) are given in Parentheses

Vibrational Frequency	1603 cm^{-1}		1360 cm^{-1}		1200/1245 cm^{-1}	
Solvent	t_1, ($\tau_{b\text{-}ET}$[17,18])/ps	t_2/ps	t_1/ps	t_2/ps	t_1/ps	t_2/ps
PC	1.0 ± 0.3, (1.1)	6.1 ± 0.4	3.0 ± 0.5	5.0 ± 0.6	Nonexp.	5.3 ± 1.2
GTA	3.8 ± 0.8, (3.5)	8.5 ± 1	5.0 ± 1.2	6.7 ± 1.2	7.0 ± 1.3	7.5 ± 1.7
ETH	5.6 ± 1.2, (6.1)	5.6 ± 1.3	7.0 ± 1.4	7.0 ± 1.4	7.1 ± 1.5	7.0 ± 1.6

al level being mainly observed by anti Stokes Raman scattering with a decay time t_2, and the lowest vibrational level of the electronic ground state.

A fit of the experimental data according to this simplest possible model considering deconvolution of the cross correlation function of the pump and probe pulses results in rise and decay times, t_1 and t_2, of the corresponding vibrational levels, that clearly indicate mode selective excitation. The time constants for the vibrations at 1603 cm^{-1}, 1360 cm^{-1} and 1200/1245 cm^{-1} for B-30 dissolved in PC, GTA, and EtOH are collected in Table 1.[26]

For comparison, b-ET times ($\tau_{b\text{-}ET}$) obtained from transient absorption measurements by Barbara and co-workers are included in parentheses in the first column of Table 1.[17,18] As can be seen from Table 1 rise times t_1 vary for different modes and solvents. Mode selectivity is most pronounced for B-30 in PC. The mode with the highest observed vibrational frequency at 1603 cm^{-1} exhibits the shortest rise time of $t_1 \leq 1$ ps, that is it builds up within the time resolution of the experiment. For the vibration at 1360 cm^{-1}, a rise time of $t_1 = 3$ ps is determined. The intensity of the Raman band at 1200/1245 cm^{-1} increases even more delayed, but does not follow simple single exponential kinetics. All vibrational modes, within our experimental uncertainties, decay single exponentially with a time constant of $t_2 = 5$ ps. For B-30 dissolved in GTA, the temporal rises of the anti-Stokes Raman intensities are slower than in PC solution. Furthermore, mode selectivity is less pronounced in GTA solution than for B-30 in PC. The decay of anti-Stokes Raman intensities is somewhat slower in GTA and in EtOH solution compared to B-30 dissolved in PC.

In all solvents the rise time of the 1603 cm^{-1} mode is close to the b-ET time. This suggests predominant direct vibrational excitation of this mode by b-ET. In contrast, modes of lower frequencies are less effective accepting modes and we have to assume indirect channels of IVR. However, the almost identical decay times of the modes indicate inefficient direct transfer from the 1603 cm^{-1} mode to other strong Raman active high-frequency modes. Instead, other indirect channels of IVR have to be assumed. Consequently, modes being not observable in our experiment are expected to play an essential role in the vibrational kinetics. Unfortunately, the experimental data are not yet sufficient to determine these other pathways of IVR more in detail.

The predominant direct excitation of a mode with the highest vibrational frequency and a strong Franck–Condon factor is suggested by a simple model based on Fermi's Golden Rule.[27–30] It predicts that the transfer is most favorable for modes with strong origin shifts z, which bridge the energy gap with a minimum of quanta n.

Because of strong stray light we were not able to measure pump induced anti-Stokes bands below 400 cm^{-1} where the modes with the highest origin shifts are located. In particular, the low-frequency mode at 133 cm^{-1} might be an efficient accepting mode as well.

Less pronounced differences in the rise times of the various vibrational bands are expected for the case that b-ET times are comparable to the time scale of IVR. This is the case for B-30 in GTA and EtOH (see Table 1). Here, IVR processes strongly influence the observed rise times for all modes. Thus, these data clearly demonstrate the transition from a mode-specific behavior of B-30 in PC to IVR-dominated vibrational dynamics of B-30 in EtOH.

5. Excited Vibrational Populations. Vibrational excess populations have been derived by dividing the anti-Stokes Raman intensities by the corresponding relative Raman cross sections, which, in turn, have been calculated from the Stokes Raman intensities recorded at 300 nm. In Fig. 7 relative vibrational populations at different delay times are shown for B-30 in PC (left) and GTA (right). It is obvious that for all solvents vibrational populations deviate substantially from thermal equilibrium within the first few picoseconds. For delay times of 1.5 ps, 3 ps and for B-30 in GTA at 7.5 ps one finds smaller populations of low-frequency than of high-frequency modes, in contrast to equilibrium (Bose–Einstein) statistics. For instance, the population of the mode at 1360 cm^{-1} exceeds the 1200/1245 cm^{-1} mode population. This finding reflects the incomplete randomization of vibrational energy among the Raman active modes indicating a relatively slow intramolecular thermalization of the vibrational manifold on a picosecond time scale.

At delay times longer than about 10 ps, the vibrational populations n_j of this subgroup of vibrations of frequencies ω_j are close to thermal equilibrium controlled by Bose–Einstein statistics with a thermal population distribution:

$$n_j(\omega_j, T) = \left[\exp\left(\frac{\hbar\omega_j}{kT}\right) - 1\right]^{-1}$$

From the population distribution of the vibrations we determined vibrational temperatures T given in the insert of Fig. 7. At these temperatures thermal populations of vibrational levels above the first excited vibrational level are below 15% for the high-frequency modes and not significant for this estimation.[31]

For a comparison of the temperatures T derived for the subgroup of Raman active modes with the equilibrium temperature T_{equ} which is achieved in the case of random distribution over all vibrational modes (degrees of freedom) of the molecule, the temperature T_{equ} has been derived applying the

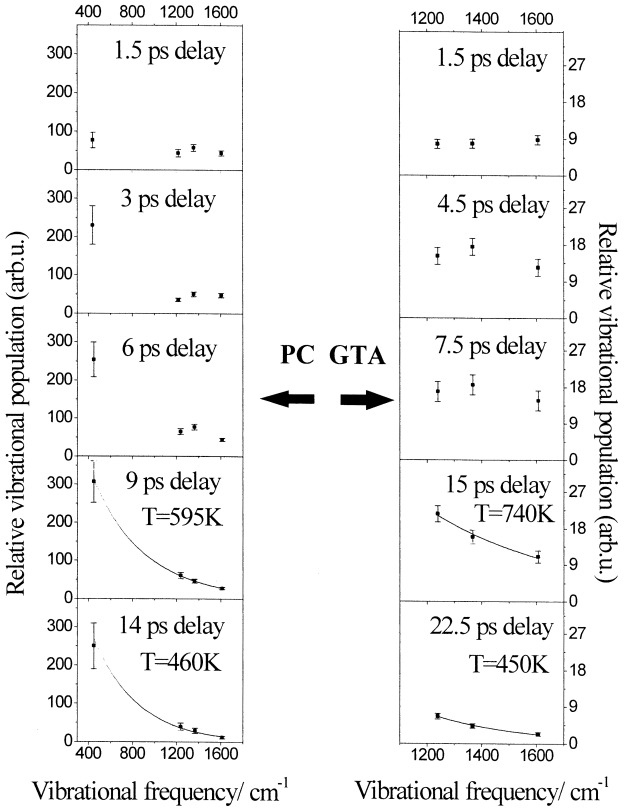

Fig. 7. Relative vibrational populations of excited vibrational levels determined for different vibrations and time delays. B-30 dissolved in PC (left). B-30 dissolved in GTA (right). Estimated temperatures at late delay times are given in the insert.

expression[32]

$$\sum_{j=1}^{3N-6}\hbar\omega_j n_j(\omega_j, T_r) + \Delta E = \sum_{j=1}^{3N-6}\hbar\omega_j n_j(\omega_j, T_{equ})$$

$\Delta E \approx 16500\ \mathrm{cm}^{-1}$ is the photon energy of the pump pulse, T_r – room temperature, and $N = 71$ is the number of atoms in the molecule. An equilibrium temperature of $T_{equ} = 520$ K has been obtained. T_{equ} represents the maximum temperature at thermal equilibrium within the complete molecule as it neglects any flow of energy to the solvent shell. This suggests that (a) b-ET transports most of the excess energy to the Raman active modes involved in the reaction, and (b) thermalization within the vibrational manifold of B-30 is incomplete even 10 to 15 ps after photoexcitation.

It is interesting to note that the measured temperatures T are higher for B-30 in GTA than for the PC solution (see insert of Fig. 7). This can be rationalized by taking into account that in the solvent controlled regime a considerable part of the absorbed energy is deposited into the solvent directly. In contrast, if the solvation time exceeds the b-ET time, a larger fraction of the initial excitation energy is randomized within the solute before dissipation to the environment becomes efficient. For B-30, solvent reorganization energies between 3000 cm^{-1} and 6000 cm^{-1} have been estimated.[5,6,18] Consequently, lower vibrational temperatures in PC compared to GTA solutions are in accordance with theoretical models of intermolecular energy transfer during b-ET in the solvent controlled regime as well as under conditions of a "frozen" solvent.

Conclusions

We obtained information about the role of vibrational modes and the main geometric changes in the process of intramolecular ET in combining stationary and time-resolved vibrational spectroscopy with ab initio calculations. The geometrical changes between electronic ground state and excited electronic states resulting from the calculations are qualitatively supported by the large origin shifts of low-frequency modes exhibiting strong contributions from torsion and *N*-pyramidalization motions, respectively. Accordingly, in B-30 the main changes of the molecular geometries induced by ET are torsional and N-inversion motions between the phenolate and pyridinium rings accompanied by some rearrangements of these rings. As torsion between the phenolate and pyridinium rings towards the perpendicular position lowers the energy gap between the S_1 and S_0 states we assign the Raman line at 133 cm^{-1} to a tuning mode.

Our investigation of vibrational populations after back-electron transfer is in agreement with expectations derived from Fermi's Golden Rule. It supports the assumption that CT resonance Raman intensities reveal the main accepting modes of ultrafast b-ET. Accordingly, strong Raman active high-frequency modes of the stationary Raman spectrum are the dominant accepting modes whereas low-frequency modes with comparable FC-factors display strong contributions from IVR processes. In addition low-frequency tuning modes with very high FC-factors may also be effective in accepting energy directly.

Ultrafast b-ET of B-30 results in non-equilibrium vibrational populations in the first few picoseconds. This points to a rather slow redistribution of vibrational energy in this relatively large molecule. Enhanced vibrational temperatures of Raman active modes support their dominance as accepting modes in the b-ET process. Vibrational temperatures of B-30 are lower in fast relaxing solvents than in slowly relaxing solvents, probably because of fast solvation in the excited electronic state for solvent controlled b-ET.

We thank the "Deutsche Forschungsgemeinschaft" for financial support. J. D. gratefully acknowledges a fellowship of the "Deutsche Forschungsgemeinschaft." A. V. thanks the "International Bureau of the BMBF" of Germany for financial support.

References

1 M. Klessinger and J. Michl, "Excited States and Photochemistry of Organic Molecules," VCH Publishers, New York (1995).

2 Special issue, *Chem. Phys.*, **259** (2000).

3 W. Domcke and G. Stock, "Adv. in Chem. Phys.," ed by I. Prigogine and S. A. Rice, **100**, 1 (1997).

4 A. B. Myers and R. A. Mathies, "Biological Applications of Raman Spectroscopy, Vol. 2," ed by T. G. Spiro, John Wiley & Sons, (2001).

5 Y. Zong and J. L. McHale, *J. Chem. Phys*., **106**, 4963 (1997).

6 Y. Zong and J. L. McHale, *J. Chem. Phys*. **107**, 2920 (1997).

7 M. Lillichenko, D. Tittelbach-Helmrich, J. W. Verhoeven, I. R. Gould, and A. B. Myers, *J. Chem. Phys*., **109**, 10958 (1998).

8 A. M. Moran and A. Myers Kelley, *J. Chem. Phys*., **115**, 912 (2001).

9 J. Quin, S. L. Schultz, and J. Jean, *Chem. Phys. Lett*., **233**, 9 (1995).

10 P. Matousek, A. W. Parker, W. T. Toner, M. Towrie, D. L. A. de Faria, R. Hester, and J. N. Moore, *Chem. Phys. Lett*., **237**, 471 (1995).

11 "Electron Transfer From Isolated Molecules To Biomolecules," Parts 1 and 2 Advances in Chemical Physics, ed by M. Bixon and J. Jortner, Wiley, New York, Vol. **106** and **107** (1999).

12 P. Y. Chen and T. J. Meyer, *Chem. Rev*., **98**, 1439 (1998).

13 P. F. Barbara, T. J. Meyer, and M. A. Ratner, *J. Phys. Chem*., **100**, 13148 (1996).

14 W. Liptay, B. Dumbacher, and H. Weisenberger, *Z. Naturforschung A*, **23**, 1613 (1968).

15 C. Reichardt, in "Molecular Interactions, Vol. 3," ed by H. Ratajczak and W. J. Orville-Thomas, Wiley, New York, 241 (1982).

16 E. Akesson, G. C. Walker, and P. F. Barbara, *J. Chem. Phys*., **95**, 4188 (1991).

17 A. E. Johnson, N. E. Levinger, W. Jarzeba, R. Schlief, D. A. V. Kliner, and P. F. Barbara, *Chem. Phys*., **176**, 555 (1993).

18 G. C. Walker, E. Akesson, A. E. Johnson, N. E. Levinger, and P. F. Barbara, *J. Phys. Chem*., **96**, (1992) 3728.

19 J. Lobaugh and P. Rossky, *J. Phys. Chem. A*, **103**, 9432 (1999).

20 S. Hogiu, W. Werncke, M. Pfeiffer, and T. Elsaesser, *Chem. Phys. Lett*., **312**, 407 (1999).

21 A. I. Vodchits, W. Werncke, S. Hogiu, and V. A. Orlovich, *Proc. SPIE*, **4352**, 53 (2001)

22 M. J. Frisch, G. W. Trucks, H. B. Schlegel, G. E. Scuseria, M. A. Robb, J. R. Cheeseman, V. G. Zakrzewski, J. A. Montgomery, R. E. Stratmann, J. C. Burant, S. Dapprich, J. M. Millam, A. D. Daniels, K. N. Kudin, M. C. Strain, O. Farkas, J. Tomasi, V. Barone, M. Cossi, R. Cammi, B. Mennucci, C. Pomelli, C. Adamo, S. Clifford, J. Ochterski, G. A. Petersson, P. Y. Ayala, Q. Cui, K. Morokuma, D. K. Malick, A. D. Rabuck, K. Raghavachari, J. B. Foresman, J. Cioslowski, J. V. Ortiz, B. B. Stefanov, G. Liu, A. Liashenko, P. Piskorz, I. Komaromi, R. Gomperts, R. L. Martin, D. J. Fox, T. Keith, M. A. Al-Laham, C. Y. Peng, A. Nanayakkara, C. Gonzalez, M. Challacombe, P. M. W. Gill, G. B. Johnson, W. Chen, M. W. Wong, J. L. Andres, M. Head-Gordon, E. S. Replogle, and J. A. Pople, "Gaussian 98 (Revision A.2)," Gaussian, Inc., Pittsburgh PA (1998).

23 W. Bartkowiak and Lipinski, *J. Phys. Chem. A*, **102**, 5236 (1998).

24 S. Hogiu, J. Dreyer, M. Pfeiffer, K. W. Brzezinka, and W. Werncke, *J. Raman Spectrosc*., **31**, 797 (2000).

25 P. G. Jasien and L. L. Weber, *J. Mol. Struct. (Theochem)*, **572**, 203 (2001)

26 S. Hogiu, W. Werncke, M. Pfeiffer, J. Dreyer, and T. Elsaesser, *J. Chem. Phys*., **113**, 1587 (2000).

27 J. Jortner and M. Bixon, *J. Chem. Phys*., **88**, 167 (1988).

28 M. Bixon and J. Jortner, *J. Chem. Phys*., **176**, 467 (1993).

29 K. Wynne, C. Galli, and R. M. Hochstrasser, *J. Chem. Phys*., **100**, 4797 (1994).

30 K. Wynne, G. D. Reid, and R. M. Hochstrasser, *J. Chem. Phys*., **105**, 2287 (1996).

31 S. Wachsmann-Hogiu, W. Werncke, J. Dreyer, A. I. Vodchits, K. W. Brzezinka, and T. Elsaesser, *Recent Res. Devel. Chem. Physics*, **2**, 61 (2001).

32 T. Nakabayashi, H. Okamoto, and M. Tasumi, *J. Phys. Chem. A*, **101**, 3494 (1997).